Molecular orbital cluster calculation study of electron correlation and local lattice instability in $La_{2-2x}Sr_{1+2x}Mn_2O_7$

Satoru Miyaki, Shinji Uzuhara, Kazuto Terada, and Kenji Makoshi
Graduate School of Material Science, University of Hyogo, Kamigori, Ako-gun, Hyogo 678-1297, Japan

Hiroyasu Koizumi*
Institute of Materials Science, University of Tsukuba, Tsukuba, Ibaraki 305-8573, Japan
(Received 26 July 2004; published 24 February 2005)

In order to examine covalence and polaron effects in the bilayer manganite $La_{2-2x}Sr_{1+2x}Mn_2O_7$, we have performed molecular orbital cluster calculations. Two types of $(Mn_2O_{11})^{15-}$ clusters, one with the manganese aligned in the *a* direction and the other in the *c* direction, were embedded in a point charge environment that mimicked the crystal environment of the bilayer manganite at $x=0.40$, and their electronic states were calculated by the unrestricted Hartree-Fock (UHF) and the complete active-space self-consistent field (CASSCF) methods. The CASSCF result for the cluster along the *a* direction exhibits double-well potential energy surfaces for symmetry-breaking deformations. This indicates small polaron formation in this system. On the other hand, the UHF calculation did not give double-well potential surfaces, showing the importance of the electron correlation for the polaron formation. Significantly large wells are obtained for the in-plane antiphase breathing and in-plane antiphase O—Mn—O stretching deformations. The double-well barrier for the former is 68 meV and that for the latter is 92 meV, where the former is close to the experimentally obtained polaron hopping activation energy above T_c. A similar calculation for the cluster along the *c* direction exhibits a negligibly small double well, indicating that the polaron effect is very small in the carrier hopping in the *c* direction within a bilayer. Electronic structures have been investigated using natural orbitals. At a double-well minimum, a localized polaron orbital is seen. In the ground state, a small but significant hole population is found in *p* orbitals of the bridging oxygen, and a slight electron population is found in the e_g orbital above the localized polaron orbital. For the cluster along the *a* direction and without deformation, the first excited state is an electron-transfer state where an electron is moved from the bridging oxygen p_z to a manganese e_g orbital. This excited state couples with the ground state by the pseudo-Jahn-Teller effect, thus, the polaron is the "pseudo-Jahn-Teller polaron." Using the natural orbitals, we have calculated magnetic Compton profiles and compared with experiment. Comparison between the experimental and theoretical results suggests the presence of polarons below T_c. We briefly discuss the implication of this result in relation to the colossal magnetoresistance effect.

DOI: 10.1103/PhysRevB.71.085117 PACS number(s): 71.10.−w, 75.47.Lx, 31.15.Ar, 13.60.Fz

I. INTRODUCTION

Anomalous electric conductivity in various transition metal oxides is currently drawing considerable attention.[1] Strong electron correlation caused by large Coulomb repulsion at transition metal sites is believed to be crucial for observed anomalous conductivity, magnetism, and superconductivity. The covalence effect within each metal-oxygen complex is also certainly important. Its importance is manifested in experimental observations in cuprates[2] and manganites,[3] where a significant amount of doped holes are found in oxygen orbitals, and band gaps for those materials without doping are due to the charge transfer within the metal-oxygen cluster.[4] Theoretical investigations are usually performed on models that do not explicitly include oxygen orbitals,[5] but the validity of such a treatment has not been sufficiently investigated. In the present work, we will fill this gap by examining the importance of those usually neglected orbitals in the colossal magnetoresistive manganite $La_{2-2x}Sr_{1+2x}Mn_2O_7$.

Historically, the covalence effect was introduced as a correction from the metal-ligand bonding effect on ionic metal-ligand interaction.[6] An accurate description of the covalency often requires more than one electronic configuration.[7] This occasionally leads to the appearance of several energy minima at different atomic configurations,[8] thus, local lattice instability is a common phenomenon in metal-ligand systems. To some extent, a transition metal oxide crystal can be viewed as a periodic array of metal-ligand complexes; therefore, the covalence effect is expected to play a role. Indeed, polaron formation associated with local lattice instability has been indicated in $La_{2-2x}Sr_{1+2x}Mn_2O_7$,[9–11] and it is thought to be relevant to short-range charge ordering,[12] pseudogap phenomena,[13–15] and the colossal magnetoresistance (CMR) effect.

In order to examine lattice instability and polaron formation in the manganese oxide, we have performed molecular orbital cluster calculations. This method should be considered as a complementary method to the band calculation based on the density functional theory (DFT). Although band calculations give useful information about the electronic state of $La_{2-2x}Sr_{1+2x}Mn_2O_7$,[13,16,17] they cannot explain some important experimental findings such as the pseudogap phenomenon.[13–15] This may be related to the fact that the

present DFT methodology is still not capable of sufficiently taking into account electron correlation effects. In this respect the molecular orbital method has an advantage; it can systematically include electron correlations. Thus, if sufficiently elaborated calculations are performed, accurate results will be obtained. However, such calculations for bulk systems are still not feasible; instead, cluster calculations are usually performed. The cluster calculations have been successfully utilized in many situations: molecular orbitals obtained by the *ab initio* cluster calculation are used in interpreting magnetic Compton profile measurements;[18] semiempirical cluster calculations have been used to reproduce observed experimental spectra.[2–4,19] Therefore, it is expected that the molecular orbital cluster calculation on the bilayer manganite $La_{2-2x}Sr_{1+2x}Mn_2O_7$ will give useful information about anomalous conductivity phenomena.

In the study of the CMR effect, the bilayer manganite $La_{2-2x}Sr_{1+2x}Mn_2O_7$ occupies a special place[20] because it cleaves very well at the rocksalt layer between MnO_2 bilayers. Thus, it is suitable for angle-resolved photoemission spectroscopy (ARPES) measurements. The electronic state revealed by ARPES experiments is remarkable, showing a pseudogap and a ghost Fermi surface (FS).[13–15] A pseudogap is also observed in the high-T_c cuprate, but unlike the cuprate case, this pseudogap extends over the entire FS and exists both above and below T_c.[14] The ghost FS is another mystery. It seems like a prototypical metallic FS characterized by the usual transport parameters.[21] However, its spectral weight is unusually low, and the resistivity calculated with experimentally estimated transport parameters is one order of magnitude smaller than the experimental value. It also exhibits portions parallel to the *a* or *b* axis, that remind us of the stripelike charge order observed in the cuprate.[15] The origin of the pseudogap was argued to be charge density wave (CDW) state formation;[15] however, this interpretation is incompatible with the observation that the current above T_c is due to polarons.[9,11] As will be seen later, the present work suggests the presence of polarons even below T_c, and this may be the key to understanding the anomalous ARPES result.

In the following, we first present results for single manganese clusters $(MnO_6)^{8-}$ and $(MnO_6)^{9-}$ embedded in a point charge distribution that mimics the crystal environment. Then, the result for two types of $(Mn_2O_{11})^{15-}$ clusters, one with the manganese aligned in the *a* direction and the other in the *c* direction, are examined. In order to investigate local lattice instability, the total energies have been calculated with changing atomic positions. The electronic states are examined with natural orbitals. Then, the magnetic Compton profile (MCP) is calculated and compared with the experimental one. The excellent agreement between theory and experiment suggests the presence of polarons below T_c. Finally, we discuss the implication of the present results with respect to the electric conduction, pseudogap, and CMR effect in the manganite.

II. MnO_6 CLUSTER

In this section, we consider single manganese clusters, $(MnO_6)^{8-}$ and $(MnO_6)^{9-}$, embedded in a point charge environment. We have previously reported results for the same clusters in a different environment where each surrounding oxygen next to the cluster was replaced by a sum of a point charge (for the manganese nucleus) and a charge distribution (for electrons for Mn^{+3} ion).[22] In the following sections, point charges +3 will be used for manganese adjacent to the cluster, therefore, we report the single manganese results in the same environment here for the comparison sake.

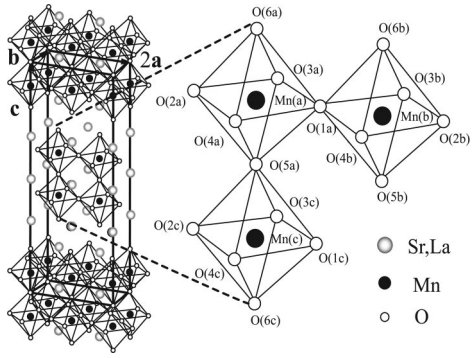

FIG. 1. The crystal structure of $La_{2-2x}Sr_{1+2x}Mn_2O_7$. The space group is $I4/mmm$. Structure parameters used are $a=3.8645$ Å; $c=20.065$ Å; Mn (0,0,0.096); La, Sr(1) (0,0,0.5); La, Sr(2) (0,0,0.317); O(1) (0,0,0); O(2) (0,0,0.19668); O(3) (0.5,0,0.096) (Ref. 23).

In the following the crystal structure for $x=0.4$ at 10 K was employed[23] with neglect of slight buckling of oxygens out of the *a*-*b* plane (Fig. 1). The details of the calculations were similar to our previous work:[22,24] the crystal environment was mimicked by point charges placed at atomic positions in the $3\times3\times3$ units of the $\mathbf{a}\cdot(\mathbf{b}\times\mathbf{c})$ rectangular parallelepiped surrounding the MnO_6 cluster with Mn(a) depicted in Fig. 1. The stoichiometric charges for O, Sr, and La are −2, +2, and +3, respectively, but we placed +2.4 charges for both Sr and La positions assuming a random distribution of them. We also placed +3.4 for Mn positions for the similar reason. The Evjen method was employed for charges on the faces, edges, and vertices of the outermost cell. Starting orbitals for complete active-space self-consistent field (CASSCF) calculations were obtained by restricted Hartree-Fock calculations. The active space of the CASSCF calculation was composed of nine highest-energy oxygen $2p$ orbitals and five manganese $3d$ orbitals. In order to obtain wave functions and total energies, the GAMESS program package[25] was used. The basis by Schäfer *et al.* **(**Mn $(14s,9p,5d)/[8s,5p,3d]$, O $(10s,6p)/[6s,3p]$**)** was employed,[26] but we omitted the most diffuse Mn *s* basis function since it extends too much over the nearby oxygens.

First, we examine the $(MnO_6)^{9-}$ cluster. In Table I charge and spin densities obtained by CASSCF and unrestricted Hartree-Fock (UHF) calculations for the $(MnO_6)^{9-}$ cluster (the nominal charge of the manganese is +3) are listed. The densities at atomic sites are Mulliken populations. The CASSCF and UHF results are almost the same.

In order to take a close look at the electronic structure, we calculated the natural orbital basis $\{\chi_{i\sigma}\}$ that diagonalizes the spin-specified first-order reduced density matrix $\rho_\sigma(\mathbf{x},\mathbf{x}')$:[27]

TABLE I. Charge and spin densities for $(MnO_6)^{9-}$ and $(MnO_6)^{8-}$. The labels for atoms are given in Fig. 1.

	Charge (Spin) $(MnO_6)^{9-}$		Charge (Spin) $(MnO_6)^{8-}$	
Atom	CASSCF	UHF	CASSCF	UHF
Mn(a)	2.631 (3.857)	2.611 (3.889)	2.505 (3.308)	2.100 (4.866)
O(1a), O(2a)	−1.937 (0.017)	−1.925 (0.009)	−1.775 (−0.047)	−1.984 (0.008)
O(3a), O(4a)	−1.937 (0.017)	−1.925 (0.009)	−1.870 (0.030)	−1.995 (0.025)
O(5a)	−1.933 (0.046)	−1.950 (0.046)	−1.321 (−0.292)	−1.059 (−0.967)
O(6a)	−1.949 (0.030)	−1.962 (0.028)	−1.892 (0.017)	−1.086 (−0.964)

$$\rho_\sigma(\mathbf{x},\mathbf{x}') = \sum_{i,\sigma} n_{i\sigma}\chi^*_{i\sigma}(\mathbf{x})\chi_{i\sigma}(\mathbf{x}'), \quad (1)$$

where $n_{i\sigma}$ is the occupation number for the natural orbital $\chi_{i\sigma}$. The natural orbitals and their occupation numbers are tabulated in Table II. All the occupation numbers are essentially integral, showing the smallness of the electron correlation. The highest occupied orbital is the $d_{3z^2-r^2}$ orbital, i.e., the $3z^2-r^2$ type E_g orbital.

The first excited state was also calculated although the result is not tabulated. It also indicates the smallness of the correlation effect. Its electronic configuration is very simple. It is basically obtained from that of the ground state by promoting an electron from the $d_{3z^2-r^2}$ orbital to $d_{x^2-y^2}$. The lattice instability study indicates that this is a typical $E\otimes e$ Jahn-Teller system.[24] Overall, the $(MnO_6)^{9-}$ cluster (corresponds to Mn^{3+} in the usual model[5]) is accurately described with a single configuration. This result is consistent with the usual model treatment for Mn^{3+}.

Now, we consider the $(MnO_6)^{8-}$ cluster. By introducing a hole in the $(MnO_6)^{9-}$ cluster, the $(MnO_6)^{8-}$ cluster (the nominal charge on the manganese is +4) is obtained. In contrast to the $(MnO_6)^{9-}$ cluster, it exhibits significant electron correlation effects. We first note that the spin contamination is quite large in the UHF result; the calculated total spin is $S=1.946$, although it should be $S=1.5$. The charge and spin densities calculated by the CASSCF and UHF methods are significantly different as seen in Table I. The doped hole is mainly in O(5a) in the CASSCF calculation, but in O(5a) and O(6a) in the UHF calculation. Many occupation numbers for the natural orbitals tabulated in Table II are fractional, indicating the strong correlation effect. The doped hole is mainly in the 39th O(5a) p_x orbital. Actually, the ground state of the $(MnO_6)^{8-}$ cluster is doubly degenerate due to two possibilities in the doped hole position, one in the O(5a) p_x orbital and the other in the O(5a) p_y orbital.[24] Overall, the $(MnO_6)^{8-}$ cluster (corresponding to Mn^{4+} in the usual model[5]) cannot be described by a single configuration. Configurations with holes in oxygen orbitals are also important. This contradicts the currently prevailing model but is consistent with the photoemission spectroscopy interpretation.[3]

III. Mn_2O_{11} CLUSTER ALONG THE *a* DIRECTION

In this section we will consider the $(Mn_2O_{11})^{15-}$ cluster with two manganese atoms [Mn(a) and Mn(b) in Fig. 1] along the *a* direction. This cluster may be viewed as a mixed-valence cluster with one Mn^{3+} and one Mn^{4+}, or as a hole-doped one in the $(Mn_2O_{11})^{16-}$ cluster. The crystal environment was taken into account by placing point charges in the $4\times3\times3$ units of the $\mathbf{a}\cdot(\mathbf{b}\times\mathbf{c})$ cell depicted in Fig. 1. Starting orbitals for CASSCF calculations were obtained by restricted Hartree-Fock calculations with $S_z=7/2$; the active orbitals were ten 3*d* orbitals for the two manganese atoms, and three 2*p* orbitals for the bridging O(1a) oxygen. We only included the three oxygen 3*p* orbitals in the active space because of practical computational limitations.

In order to investigate local lattice instability, we have calculated the total energy as a function of various deformations. We choose those deformations that are combinations of E_g-type Jahn-Teller and breathing deformations. We also considered the simple bridging oxygen shift along the *a* axis. Six deformations considered in this study are depicted in Fig. 2, together with potential energies for corresponding defor-

TABLE II. Occupation numbers and main characteristics of natural orbitals for $(MnO_6)^{9-}$ and $(MnO_6)^{8-}$.

		Occupation number $(MnO_6)^{9-}$		Occupation number $(MnO_6)^{8-}$	
Orbital number	Main characteristic	↑	↓	↑	↓
39	O(5a) p_x	1.00	1.00	0.23	0.80
40	Mn(a) d_{xy}	1.00	0.00	1.00	0.05
41	Mn(a) d_{yz}	1.00	0.00	1.00	0.05
42	Mn(a) d_{xz}	1.00	0.00	0.77	0.06
43	Mn(a) $d_{3z^2-r^2}$	1.00	0.00	0.99	0.04
44	Mn(a) $d_{x^2-y^2}$	0.00	0.00	0.01	0.00

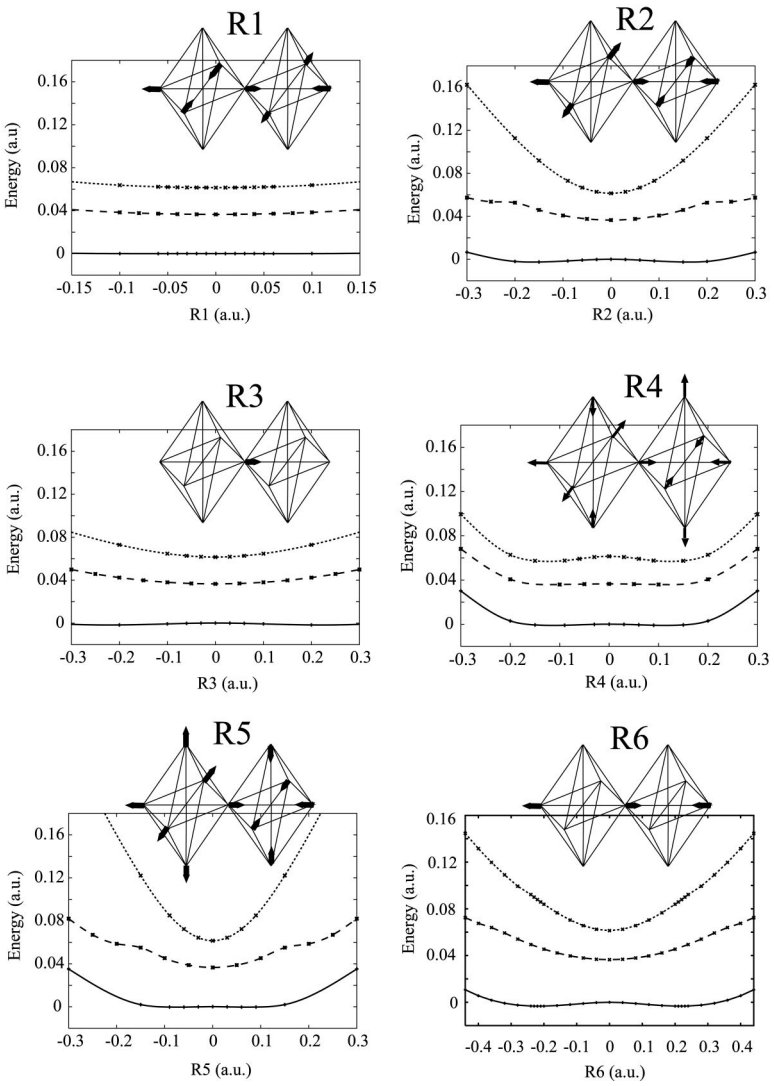

FIG. 2. Potential energies for local lattice deformations for the $(Mn_2O_{11})^{15-}$ cluster along the *a* direction. Three lines in each figure describe potential surfaces for the first excited state by the CASSCF calculation (top), for the ground state by the UHF calculation (middle), and for the ground state by the CASSCF calculation (bottom), respectively.

mations: R1 is the antiphase combination of the x^2-y^2-type Jahn-Teller deformation; R2 is the antiphase in-plane breathing mode; R3 is the O(1a) shift along the *a* axis; R4 is the antiphase combination of the $3z^2-r^2$-type Jahn-Teller deformation; R5 is the antiphase in-plane breathing mode; R6 is the antiphase in-plane O—Mn—O stretching in the *a* direction. Although the MnO_6 complexes are slightly distorted from the regular octahedron, we take atomic movements for regular octahedron. For the unit deformation for each R*i*, atoms move 1 a.u. in the directions indicated by arrows. But for the R4 deformation, long and short arrows indicate 2 and 1 a.u. moves per unit deformation, respectively.

Double-well potential surfaces were obtained in the CASSCF results for all the deformations considered as seen in Fig. 2. Contrary to the CASSCF results, the UHF results did not show double wells. This indicates that the electron correlation is crucial for double-well formation. The double well means local lattice instability and small polaron formation. Significantly deep wells are seen in the R2 and R6 deformations. The well is deepest for the R6 deformation with a barrier height of 92 meV. The barrier for the R2 deformation is 68 meV, which is very close to the experimentally obtained activation energy 65 meV for carrier hopping above T_c.[9]

In Table III, charge and spin densities are tabulated. They were calculated from the UHF and CASSCF results using the standard Mulliken population partitioning. The spin density is concentrated on the two manganese atoms, and the doped hole is mainly in the bridging oxygen. In order to examine the electronic state variation associated with polaron formation, the results for R2- and R6-deformed clusters are also listed. In those deformations the potential minima are at R2 = ±0.17 a.u. and R6 = ±0.22 a.u., respectively. The results for the UHF and CASSCF at R2 = R6 = 0 are similar, although the charge on manganese is smaller and the hole population in the bridging oxygen O(1a) is larger for the former. When the cluster is deformed charges and spin densities at two manganese sites become different. Actually, in the R6 = 0.22 result, the charges on the two manganese atoms are almost equal, although the spin density indicates that Mn(a) is in the $S_z=2$ state and Mn(b) is in the $S_z=3/2$ state.

In order to take a close look at the electronic state, natural orbitals and their occupation numbers were calculated. They are tabulated in Table IV. In general a natural orbital is a linear combination of many atomic orbitals and its characterization is not so simple; nevertheless, we attribute a main characteristic to each orbital. The orbital numbers from 1

TABLE III. The ground state charge and spin densities for the $(Mn_2O_{11})^{15-}$ cluster along the *a* direction.

	R2=R6=0 (UHF)	R2=R6=0 (CASSCF)	R2=0.17 (CASSCF)	R6=0.22 (CASSCF)
Atom	Charge (Spin)	Charge (Spin)	Charge (Spin)	Charge (Spin)
Mn(a)	2.400 (3.896)	2.508 (3.387)	2.573 (3.408)	2.426 (3.747)
Mn(b)	2.400 (3.896)	2.508 (3.387)	2.338 (3.296)	2.419 (2.879)
O(1a)	−1.081 (−0.733)	−1.283 (0.028)	−1.363 (0.100)	−1.184 (0.183)
O(2a)	−1.945 (0.047)	−1.939 (0.030)	−1.977 (0.018)	−1.997 (0.020)
O(2b)	−1.945 (0.047)	−1.939 (0.030)	−1.870 (0.040)	−1.833 (0.038)
O(3a)	−1.863 (−0.015)	−1.866 (0.017)	−1.934 (0.015)	−1.876 (0.020)
O(3b)	−1.863 (−0.015)	−1.866 (0.017)	−1.790 (0.024)	−1.850 (0.015)
O(4a)	−1.863 (−0.015)	−1.866 (0.017)	−1.934 (0.015)	−1.876 (0.020)
O(4b)	−1.863 (−0.015)	−1.866 (0.017)	−1.790 (0.024)	−1.850 (0.015)
O(5a)	−1.819 (−0.023)	−1.825 (0.022)	−1.816 (0.021)	−1.837 (0.025)
O(5b)	−1.819 (−0.023)	−1.825 (0.022)	−1.810 (0.021)	−1.805 (0.018)
O(6a)	−1.868 (−0.024)	−1.870 (0.011)	−1.865 (0.010)	−1.880 (0.013)
O(6b)	−1.868 (−0.024)	−1.870 (0.011)	−1.859 (0.010)	−1.856 (0.008)

through 70 are core orbitals for CASSCF calculations and they are doubly occupied. The orbital numbers from 74 through 79 are six t_{2g} orbitals and occupied by the majority spins. Because the hybridization between the O(1a) p_x and Mn $d_{3x^2-r^2}$ orbitals is significant and lowers the orbital energy, the $d_{3x^2-r^2}$ orbital is the lowest and most populated e_g orbital. It is also noted that a slight electron population is in the 81st orbital. The most significant difference between R2=0.17 and R6=0.22 results is that the significant hole is in the 72nd O(1a) p_x for the former but in the 73rd O(1a) p_z in the latter.

In Fig. 3, contour plots of the 72nd up-spin, 73rd up-spin, 80th up-spin, and 81st up-spin orbitals are displayed. The mixings of the bridging oxygen *p* orbitals and manganese e_g orbitals are clearly seen. In the 80th orbital, the symmetric Mn $d_{3x^2-r^2}$ orbital at R2=R6=0 becomes the localized Mn(a) e_g orbital at R2=0.17 or R6=0.22. This, together with the occupation numbers in Table IV, indicates that the 80th orbital is the polaron orbital and Mn(a) corresponds to Mn^{3+}, although the charge at Mn(a) is slightly larger than that at Mn(b). Actually, this trend is also seen in the single manganese calculations (Table I). Note that spin densities also indicate that Mn(a) and Mn(b) correspond to Mn^{3+} and Mn^{4+}, respectively. The 72nd and 81st orbitals may be viewed as the symmetric and antisymmetric combinations of the bridging oxygen p_x orbital and the manganese e_g orbitals, respectively. The 73rd orbital at R6=0.22 shows a marked difference in the p_z orbital compared with that at R2=0.17. It is

TABLE IV. Main characteristics and occupation numbers of natural orbitals for the $(Mn_2O_{11})^{15-}$ cluster along the *a* direction in the ground state. s and a in the main characteristics denote symmetric and antisymmetric combinations of two orbitals at different manganese sites, respectively.

	R2=R6=0		R2=0.17		R6=0.22	
Orbital	Main characteristics	Occupation ↑ (↓)	Main characteristics	Occupation ↑ (↓)	Main characteristics	Occupation ↑ (↓)
71	O(1a) p_y	1.00 (0.98)	O(1a) p_y	1.00 (0.99)	O(1a) p_y	1.00 (0.98)
72	O(1a) p_x	0.90 (0.91)	O(1a) p_x	0.88 (0.89)	O(1a) p_x	0.99 (0.97)
73	O(1a) p_z	0.99 (0.98)	O(1a) p_z	0.99 (0.98)	O(1a) p_z	0.93 (0.94)
74	Mn d_{yz} s	1.00 (0.00)	Mn(a) d_{yz}	1.00 (0.00)	Mn(a) d_{yz}	1.00 (0.00)
75	Mn d_{yz} a	1.00 (0.00)	Mn(b) d_{yz}	1.00 (0.01)	Mn(b) d_{yz}	0.99 (0.01)
76	Mn d_{xy} s	1.00 (0.01)	Mn(a) d_{xy}	1.00 (0.00)	Mn(a) d_{xy}	1.00 (0.00)
77	Mn d_{xz} s	1.00 (0.01)	Mn(a) d_{xz}	1.00 (0.00)	Mn(a) d_{xz}	1.00 (0.00)
78	Mn d_{xy} a	1.00 (0.01)	Mn(b) d_{xy}	1.00 (0.01)	Mn(b) d_{xy}	1.00 (0.02)
79	Mn d_{xz} a	1.00 (0.01)	Mn(b) d_{xz}	1.00 (0.01)	Mn(b) d_{xz}	1.00 (0.02)
80	Mn $d_{3x^2-r^2}$ s	0.94 (0.04)	Mn(a) $d_{x^2-y^2}$	1.00 (0.10)	Mn(a) $d_{3x^2-r^2}$	1.00 (0.00)
81	Mn $d_{3x^2-r^2}$ a	0.17 (0.04)	Mn(b) $d_{3x^2-r^2}$	0.12 (0.01)	Mn(b) $d_{3x^2-r^2}$	0.08 (0.05)
82	O(1a) p_z	0.00 (0.01)	O(1a) p_z	0.01 (0.00)	O(1a) p_z	0.01 (0.00)
83	O(1a) p_x	0.00 (0.00)	O(1a) p_x	0.00 (0.00)	O(1a) p_x	0.00 (0.00)

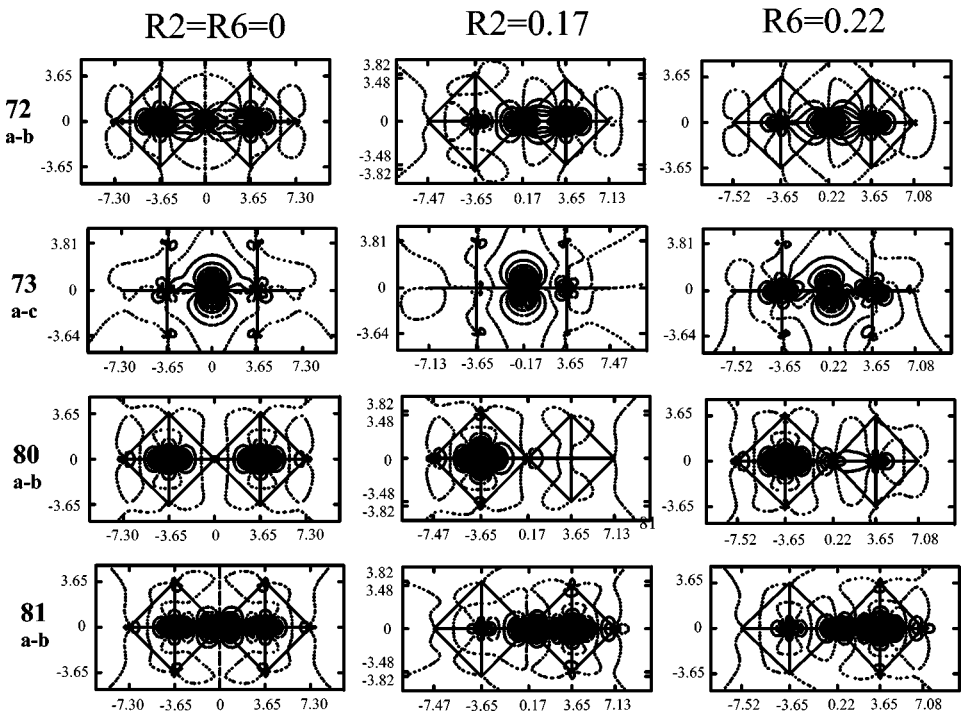

FIG. 3. Contour plots of natural orbitals for the ground state of the cluster along the *a* direction. The 72nd up-spin orbital in the *a*-*b* plane, 73rd up-spin orbital in the *a*-*c* plane, 80th up-spin orbital in the *a*-*b* plane, and 81st up-spin orbital in the *a*-*b* plane are depicted for R2=R6=0, R2=0.17, and R6=0.22.

somewhat leaning and the overlap between the p_z and manganese orbitals is increased.

In contrast to the ground state, the first excited state does not show any lattice instability as seen in Fig. 2. Charge and spin densities for the first excited state at R2=R6=0 are listed in Table V. A large hole population, more than one, is found at O(1a), and charges at manganese are significantly reduced. The occupation numbers and main characteristics of the natural orbitals are tabulated in Table VI. Almost one hole is in the O(1a) p_z. Two e_g orbitals at Mn(a) and Mn(b) are now both occupied. Actually, the ground state at R2=R6=0 is symmetric with respect to the reflection through the mirror plane located at the bridging oxygen with its normal in the *a* direction. On the other hand, the first excited state at R2=R6=0 is basically an electron-transfer state in which an electron in the bridging oxygen p_z orbital is moved to a manganese e_g orbital. Therefore the first excited state at R2=R6=0 is an antisymmetric state with respect to the same mirror reflection. This means that the double well in the ground state is actually due to the pseudo-Jahn-Teller effect,[8] where the symmetric ground state couples with the antisymmetric first excited state by antisymmetric local lattice deformations. This coupling is strong enough to cause lattice instability to form the polaron in this system.

TABLE V. Charge and spin densities for the first excited state of $(Mn_2O_{11})^{15-}$ along the *a* direction at R2=R6=0.

Atom	Charge (Spin)
Mn(a), Mn(b)	2.264 (3.590)
O(1a)	−0.748 (−0.419)
O(2a), O(2b)	−1.947 (0.038)
O(3a), O(3b), O(4a), O(4b)	−1.870 (0.020)
O(5a), O(5b)	−1.830 (0.027)
O(6a), O(6b)	−1.873 (0.014)

IV. Mn_2O_{11} CLUSTER ALONG THE *c* DIRECTION

The lattice instability was also investigated for the cluster along the *c* direction. The crystal environment was mimicked by placing point charges in the $3\times3\times3$ units of the $\mathbf{a}\cdot(\mathbf{b}\times\mathbf{c})$ cell depicted in Fig. 1. Starting orbitals for CASSCF calculations were obtained by restricted Hartree-Fock calculations with $S_z=7/2$; and the active orbitals were ten 3*d* orbitals for the two manganese, and three 2*p* orbitals for the bridging O(5a) oxygen. The result is depicted in Fig. 4 (see

TABLE VI. Occupation numbers of natural orbitals for the first excited state of $(Mn_2O_{11})^{15-}$ along the *a* direction at R2=R6=0.

Orbital	Main characteristics	Occupation ↑ (↓)
71	O(1a) p_y	1.00 (1.00)
72	O(1a) p_x	0.99 (0.99)
73	O(1a) p_z	0.11 (0.89)
74	Mn d_{yz} s	0.99 (0.01)
75	Mn d_{yz} a	0.99 (0.01)
76	Mn d_{xy} s	0.99 (0.01)
77	Mn d_{xz} s	0.97 (0.02)
78	Mn d_{xy} a	0.99 (0.01)
79	Mn d_{xz} a	0.97 (0.02)
80	Mn $d_{3x^2-r^2}$ s	0.99 (0.01)
81	Mn $d_{3x^2-r^2}$ a	0.99 (0.01)
82	O(1a) p_z	0.00 (0.00)
83	O(1a) p_x	0.01 (0.00)

TABLE VII. The ground state charge and spin densities for the $(Mn_2O_{11})^{15-}$ cluster along the *c* direction.

Atom	Charge (Spin)
Mn(a), Mn(c)	2.546 (3.372)
O(1a), O(1c)	−1.880 (0.017)
O(2a), O(2c)	−1.880 (0.017)
O(3a), O(3c)	−1.880 (0.017)
O(4a), O(4c)	−1.880 (0.017)
O(5a)	−1.184 (0.079)
O(6a), O(6c)	−1.934 (0.021)

Table VII for charge and spin densities, and Table VIII for main characteristics and occupation numbers of natural orbitals). The following deformations were considered: S1 is the O(5a) shift along the *c* axis; S2 is the antiphase combination of the $3z^2-r^2$-type Jahn-Teller deformation; S3 is the antiphase breathing mode; S4 is the antiphase breathing mode in the *b*-*c* plane; S5 is the antiphase stretching mode along the *c* axis. Although the S5 deformation shows a double-well structure, the well is negligibly shallow. In the experiment, it has been observed that the activation energy for the polaron hopping is larger in the *c* direction than that in the *a* direction. However, the present result indicates the polaron effect is negligible in the *c* direction hopping within a bilayer.[9] The experimental activation energy for the *c* direction hopping is probably due to the energy barrier for the rocksalt layer crossing between two MnO_2 bilayers. The first excited state also does not show any lattice instability as seen in Fig. 4.

V. MAGNETIC COMPTON PROFILE

In this section we compare the calculated MCP with an experimental one. The MCP is calculated using the natural orbitals from the cluster calculation as

TABLE VIII. Main characteristics and occupation numbers of natural orbitals for the $(Mn_2O_{11})^{15-}$ cluster along the *c* direction in the ground state.

Orbital number	Main characteristics	Occupation ↑ (↓)
71	O(6a) p_z	0.94 (0.90)
72	O(6a) p_x	1.00 (0.97)
73	O(6a) p_y	1.00 (0.97)
74	Mn d_{xy} s	1.00 (0.00)
75	Mn d_{xy} a	1.00 (0.00)
76	Mn d_{yz} s	1.00 (0.02)
77	Mn d_{xz} s	1.00 (0.02)
78	Mn d_{xz} a	1.00 (0.02)
79	Mn d_{yz} a	1.00 (0.02)
80	Mn $d_{3z^2-r^2}$ s	0.93 (0.04)
81	Mn $d_{3z^2-r^2}$ a	0.13 (0.04)
82	O(5a) s	0.00 (0.01)
83	O(5a) p_z	0.00 (0.00)

$$\frac{\partial^2\sigma}{\partial\Omega\partial\omega} \propto \int dp_x dp_y \sum_i [\lambda_{i\uparrow}|\hat{\chi}_{i\uparrow}(\mathbf{p})|^2 - \lambda_{i\downarrow}|\hat{\chi}_{i\downarrow}(\mathbf{p})|^2], \quad (2)$$

where $\hat{\chi}_{i\sigma}(\mathbf{p})$ is the Fourier transform of the natural orbital $\chi_{i\sigma}(\mathbf{x})$.[28]

The experimental result for the system at $x=0.42$ with the *z* axis along the [001] direction is displayed in Fig. 5. It was taken at 10 K in a 2.5 T magnetic field. This MCP was already examined using Hartree-Fock orbitals before,[18] but we reexamine it here in order to access the importance of electron correlations and polaron formation. The theoretical MCP's were obtained using the natural orbitals from the calculations for $(Mn_2O_{11})^{15-}$ cluster in the *a* direction.

The difference between theory and experiment is largest around $p_z=0$. This is partly due to the difference in the hole concentration for the theory ($x=0.5$) and experiment ($x=0.42$), and the neglect of the band effect. The correlation effect is noticeable by comparing the CASSCF result at R2=R6=0 and UHF result at R2=R6=0, where the CASSCF result has more intensity around $p_z=0$, and agrees better with experiment. The comparison of the CASSCF result at R2=R6=0 and that at R2=0.17 or R6=0.22 shows that the polaron effect increases the intensity around $p_z=0$, and improves the agreement between theory and experiment. The agreement is best for the R6=0.22 result. This suggests the existence of polarons below T_c.

VI. DISCUSSION

In the present work we have demonstrated that this system has local lattice instabilities. As a consequence, the mixed-valence pairs Mn^{3+}—O—Mn^{4+} (3+ and 4+ are nominal charges) are formed. Note that although the spins on the two manganese are $S_z=3/2$ and $S_z=2$, the charges on them are almost equal. A mixed-valence pair, the Zener pair polaron was proposed by Zhou *et al.*[9] The present work supports the formation of such pairs; however, the stabilization is not due to Zener's double-exchange interaction.[29] The Jahn-Teller instability of Mn^{3+} is certainly important since it provides a large electron-lattice coupling. However, the most significant contribution comes from the pseudo-Jahn-Teller coupling between the ground and first excited states. This coupling becomes possible due to the occupation of holes in the bridging oxygen *p* orbitals, and is related to the significant electron correlation effects found in the $(MnO_6)^{8-}$ cluster calculations.

Since the polaron stabilization energy is several times larger than k_BT_c, the polarons are formed above T_c. Indeed several experiments indicate the existence of polarons above T_c and some also below T_c.[9,10,30–33] The electron conduction above T_c is most probably due to small polaron hopping, and this explains the activation-type temperature dependence of the electric conductivity above T_c.[9,11] Indeed, the present estimate of the barrier for the R2 deformation, 68 meV, is very close to the experimental estimate 65 meV obtained from the temperature dependence of conductivity.[9] We also found another significant symmetry-breaking lattice instability for the R6 deformation with the barrier 92 meV. A recent experiment suggests that the polaron types change as temperature

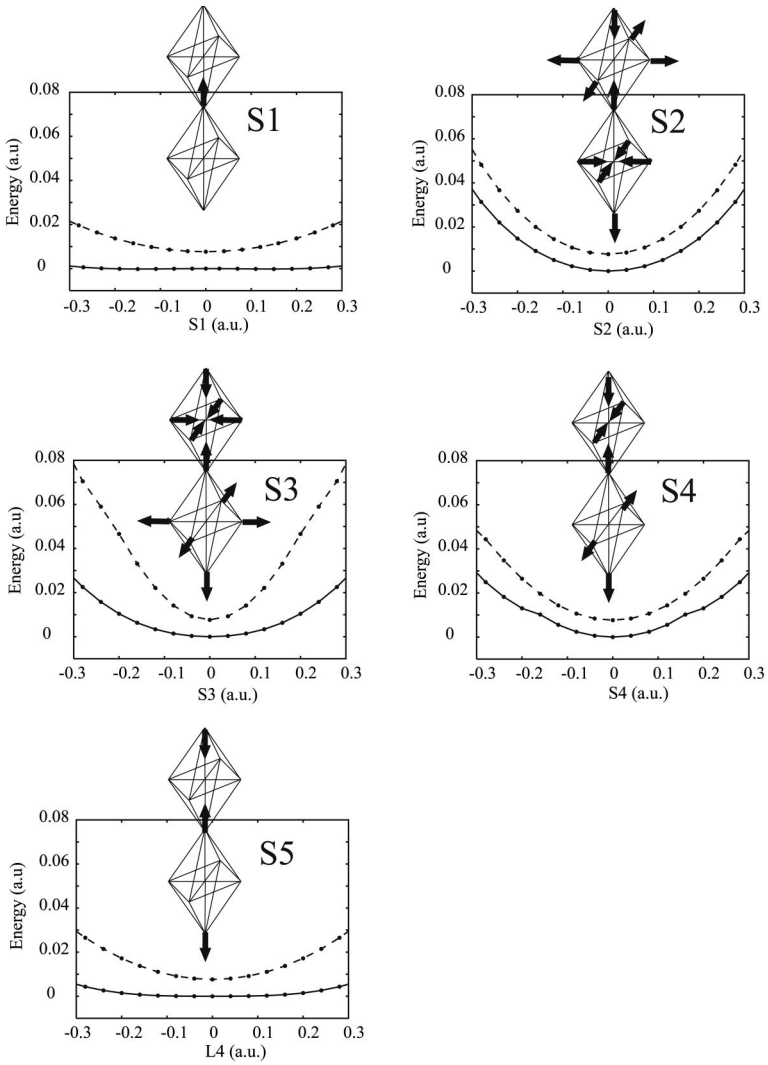

FIG. 4. Potential energies for local lattice deformations for the $(Mn_2O_{11})^{15-}$ cluster along the *c* direction. Two lines in each figure are for the first excited state by the CASSCF calculation (top) and the ground state by the CASSCF calculation (bottom), respectively.

is decreased to T_c from above.[33] This may correspond to the change from the R2 deformed polaron to the R6 deformed one.

The conduction mechanism below T_c becomes now controversial. It has been thought that it can be explained by the double-exchange mechanism for e_g band electrons since the polarons melt below T_c. The disappearance of the diffuse x-ray scattering through T_c with lowering temperature support this point of view.[10] However, the present result and a few experimental results suggest that the existence of po-

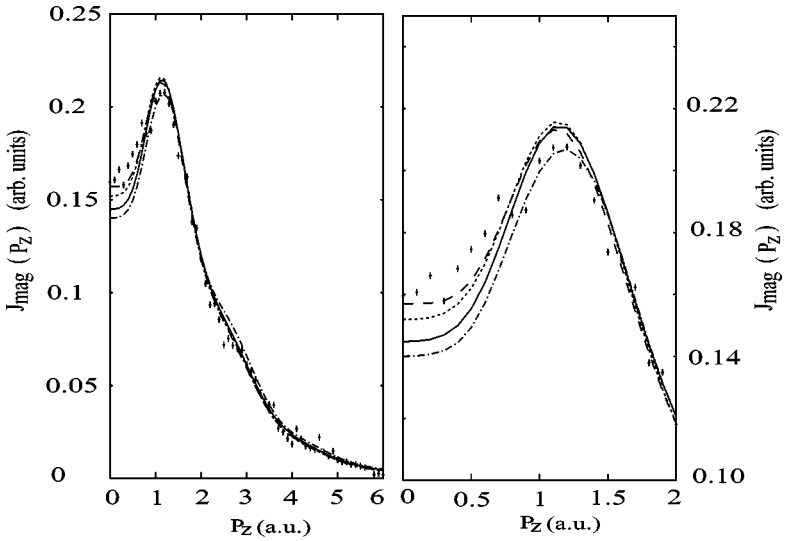

FIG. 5. Comparison of the experimental magnetic Compton profile and theoretical profiles obtained from the $(Mn_2O_{11})^{15-}$ cluster calculations. Right panel is the closeup of the left one near $p_z=0$. Pluses, experimental result; dash-dotted line, result by the UHF calculation at R2=R6=0; solid line, result by the CASSCF calculation at R2=R6=0; dotted line, result by the CASSCF calculation at R2=0.17; dashed line, result from the CASSCF calculation at R6=0.22.

larons persists below T_c.[30,31] The disappearance of diffuse scattering mentioned above may simply be interpreted as the disappearance of a disorder, and does not exclude the possibility for an appearance of a polaron order. Indeed, the ARPES experiment suggests the existence of a stripe-like order.[15] The existence of the polarons below and above T_c corresponds to the existence of a pseudogap at those temperatures.[13–15] It is also worth pointing out that contrary to common belief, a charge order does not necessarily make the system insulating. This is demonstrated in $La_{2-2x}Sr_{1+2x}Mn_2O_7$ at $x=0.5$,[34] where the CE-type charge-orbital order formation at around $T=100$ K actually reduces resistivity and the system shows metallic conductivity.

The above argument makes us surmise that the insulator-metal transition in this system may be a consequence of the disorder-order transition of the pseudo-Jahn-Teller polaron; and the CMR effect may be explained as the shift of this transition temperature by an applied magnetic field. Let us have a brief look at this possibility with a very crude model: we take the Ising model to describe this transition and employ the Bragg-Williams approximation. Then, the transition temperature is given by $T_c=zJ$ where $z=5$ is the number of nearest neighbors and J is the Ising coupling parameter. For the $x=0.4$ sample, the Curie temperature is $T_c \approx 120$ K; thus, the interaction parameter J is estimated as $J \approx 24$ K. This value is actually close to the observed value 20 K for the correlation life time for the short range antiferromagnetic correlation at $T=142$ K.[35] This suggests that the above short-range order corresponds to antiferromagnetic pseudo-Jahn-Teller polaron pairs. Such pairs should have slightly different atomic configurations compared with the ferromagnetic pairs and thus will create diffuse scattering. The polaron packing is already established well above T_c, and the final paramagnetic-ferromagnetic transition of pseudo-Jahn-Teller pairs occurs at T_c. The magnitude of the observed CMR effect corresponds to the change of J by 1.2 K per 1 T of the applied magnetic field.[20] Note that the total spin of the pseudo-Jahn-Teller polaron is rather large, $S=7/2$, and the Zeeman splitting of this spin in the magnetic field of 1 T is about 4.7 K. Thus, this scenario seems to be not unrealistic.

The present results also give some insight into the metallic conductivity below T_c. If we take the pseudo-Jahn-Teller pairs as the basic building blocks of the electronic state, a periodic arrangement of them may give rise to a conduction band composed of the 81st natural orbitals. This "split-off band" from the lower energy band due to the electron correlation may account for the metallic conductivity below T_c and also the ghost FS observed in the ARPES measurements.[13] The coexistence of the polaron and conduction bands below T_c has recently been considered by Ramakrishnan *et al.*[36] They have argued that the coexistence of the polaron and conduction bands systematically explains the CMR effect. Although their model is different from ours in detail, it seems that the coexistence scenario is promising. Note that the formation of the ordered polaron phase also means phase separation into the pair ordered phase and the rest.[5]

VII. CONCLUSION

In the present work, molecular orbital calculations have been performed on $(Mn_2O_{11})^{15-}$ clusters by the UHF and the CASSCF methods. The CASSCF result exhibits double-well potential energy surfaces for symmetry-breaking deformations. The wells are significantly large for two types of deformations, the R2 and R6 deformations depicted in Fig. 2. The excellent agreement between the experimental and theoretical MCP's sindicates the presence of polarons below T_c. It is suggested that pseudogaps may be due to polaron formation, and the split-off band above the polaron band may explains the metallic conductivity below T_c.

*Electronic address: koizumi@ims.tsukuba.ac.jp

[1] M. Imada, A. Fujimori, and Y. Tokura, Rev. Mod. Phys. **70**, 1039 (1998).
[2] A. Fujimori, E. Takayama-Muromachi, Y. Uchida, and B. Oki, Phys. Rev. B **35**, 8814 (1987).
[3] T. Saitoh, A. E. Bocquet, T. Mizokawa, H. Namatame, A. Fujimori, M. Abbate, Y. Takeda, and M. Takano, Phys. Rev. B **51**, 13 942 (1995).
[4] J. Zaanen, G. A. Sawatzky, and J. W. Allen, Phys. Rev. Lett. **55**, 418 (1985).
[5] E. Dagotto, *Nanoscale Phase Separation and Colossal Magnetoresistance* (Springer, Berlin, 2003).
[6] R. G. Shulman and S. Sugano, Phys. Rev. Lett. **7**, 157 (1961).
[7] S. Sugano and Y. Tanabe, J. Phys. Soc. Jpn. **20**, 1155 (1965).
[8] I. B. Bersuker and V. Z. Polinger, *Vibronic Interactions in Molecules and Crystals* (Springer, Berlin, 1989).
[9] J.-S. Zhou, J. B. Goodenough, and J. F. Mitchell, Phys. Rev. B **58**, R579 (1998).
[10] L. Vasiliu-Doloc, S. Rosenkranz, R. Osborn, S. K. Sinha, J. W. Lynn, J. Mesot, O. H. Seeck, G. Preosti, A. J. Fedro, and J. F. Mitchell, Phys. Rev. Lett. **83**, 4393 (1999).
[11] T. Ishikawa, K. Tobe, T. Kimura, T. Katsufuji, and Y. Tokura, Phys. Rev. B **62**, 12 354 (2000).
[12] M. Kubota, Y. Oohara, H. Yoshizawa, H. Fujioka, K. Shimizu, K. Hirota, Y. Moritomo, and Y. Endoh, J. Phys. Soc. Jpn. **69**, 1986 (2000).
[13] D. S. Dessau, T. Saitoh, C.-H. Park, Z.-X. Shen, P. Villella, N. Hamada, Y. Moritomo, and Y. Tokura, Phys. Rev. Lett. **81**, 192 (1998).
[14] T. Saitoh, D. S. Dessau, Y. Moritomo, T. Kimura, Y. Tokura, and N. Hamada, Phys. Rev. B **62**, 1039 (2000).
[15] Y.-D. Chuang, A. D. Gromko, D. S. Dessau, T. Kimura, and Y. Tokura, Science **292**, 1509 (2001).
[16] P. K. de Boer and R. A. de Groot, Phys. Rev. B **60**, 10 758 (1999).
[17] X. Y. Huang, O. N. Mryasov, D. L. Novikov, and A. J. Freeman, Phys. Rev. B **62**, 13 318 (2000).
[18] A. Koizumi, S. Miyaki, Y. Kakutani, H. Koizumi, N. Hiraoka, K. Makoshi, N. Sakai, K. Hirota, and Y. Murakami, Phys. Rev. Lett. **86**, 5589 (2001).
[19] L. C. Davis, Phys. Rev. B **25**, 2912 (1982).
[20] Y. Moritomo, A. Asamitsu, H. Kuwahara, and Y. Tokura, Nature

(London) **380**, 141 (1996).
[21] B. Keimer, Science **292**, 1498 (2001).
[22] S. Miyaki, H. Koizumi, and K. Makoshi, Chem. Phys. Lett. **350**, 359 (2001).
[23] M. Kubota, H. Fujioka, K. Hirota, K. Ohyama, Y. Moritomo, H. Yoshizawa, and Y. Endoh, J. Phys. Soc. Jpn. **69**, 1606 (2000).
[24] S. Uzuhara, H. Koizumi, S. Miyaki, and K. Makoshi, Chem. Phys. Lett. **358**, 29 (2002).
[25] M. W. Schmidt *et al.*, J. Comput. Chem. **14**, 1347 (1993).
[26] A. Schäfer, C. Huber, and R. Ahlrichs, J. Chem. Phys. **100**, 5829 (1994).
[27] P. O. Löwdin, Phys. Rev. **97**, 1474 (1955).
[28] L. Mendelsohn and V. H. Smith, in *Comton Scattering*, edited by B. Williams (McGraw-Hill, New York, 1977), p. 102.
[29] C. Zener, Phys. Rev. **82**, 403 (1951).
[30] D. Louca, T. Egami, E. L. Brosha, H. Röder, and A. R. Bishop, Phys. Rev. B **56**, R8475 (1997).
[31] C. Meneghini, C. C. S. Mobilio, A. Kumar, S. Ray, and D. D. Sarma, J. Phys.: Condens. Matter **14**, 1967 (2002).
[32] A. Daoud-Aladine, J. Rodríguez-Cavajal, L. Pindard-Gaudart, M. T. Fernández-Díaz, and A. Revcolevschi, Phys. Rev. Lett. **89**, 097205 (2002).
[33] B. J. Campbell, S. K. Sinha, R. Osborn, S. Rosenkranz, J. F. Mitchell, D. N. Argyriou, L. Vasiliu-Doloc, O. H. Seeck, and J. W. Lynn, Phys. Rev. B **67**, 020409 (2003).
[34] T. Kimura, R. Kumai, Y. Tokura, J. Q. Li, and Y. Matsui, Phys. Rev. B **58**, 11 081 (1998).
[35] T. G. Perring, G. Aeppli, Y. Moritomo, and Y. Tokura, Phys. Rev. Lett. **78**, 3197 (1997).
[36] T. V. Ramakrishnan, H. R. Krishnamurthy, S. R. Hassan, and G. V. Pai, Phys. Rev. Lett. **92**, 157203 (2004).